

Sorting Methods and Adaptive Thresholding for Histogram Based Reversible Data Hiding

Ammar Mohammadi ¹, Mansour Nakhkash ^{2*}

¹ Department of Electrical Engineering, Yazd University, Yazd, Iran

² Department of Electrical Engineering, Yazd University, Yazd, Iran

* E-mail: nakhkash@yazd.ac.ir

Abstract: This paper presents a histogram based reversible data hiding (RDH) scheme, which divides image pixels into different cell frequency bands to sort them for data embedding. Data hiding is more efficient in lower cell frequency bands because it provides more accurate prediction. Using pixel existence probability in some pixels of ultra-low cell frequency band, another sorting is performed. Employing these two novel sorting methods in combination with the hiding intensity analysis that determines optimum prediction error, we improve the quality of the marked image especially for low embedding capacities. In effect, comparing to existent RDH algorithms, the hiding capacity is increased for a specific level of the distortion for the marked image. Experimental results confirm that the proposed algorithm outperforms state of the art ones

1. Introduction

Data hiding is referred to embedding data in a cover medium such as audio, multimedia, image, and textual files. Embedding data in image has many applications, among them are copy right protection, authentication, cover communication, and so on. The cover image is, usually, distorted in many applications of data hiding, and the original cover cannot be restored. However, there exist applications in medical image sharing, multimedia archive management and so on, which needs the restoration of the cover without any distortion. Reversible data hiding (RDH) is an approach that addresses the methods for complete restoration of the original cover after the extraction of embedded data.

There are various methods in RDH [1]; but the more developed methods can be classified into two main categories: The methods based on DE (difference expansion) [2] and histogram modification [3]. Novel methods in RDH employ prediction-error expansion [4]–[10], that is pioneered in [11], lossless compression [12]–[16] that are based on [17] scheme, code division multiplexing [18] and prediction-error modification [19]–[24], mostly in combination with two main DE and histogram based techniques.

The difference expansion (DE) is proposed by Tian [2] in 2003. In DE, the image is divided into pairs of pixels, in which the data bits are embedded. This method embeds one bit into a pixel pair and thus a hiding rate up to 0.5 bit per pixel can be realized. Tian exploits a location map to record the selected expandable locations, where the difference of pixel pairs is small enough to make less distortion. Location maps, usually, are enormous in size occupying a notable portion of the payload. Kamstra *et al.* [25] outperform the method of [2] by sorting pixel pairs according to the local variance. The basic idea of sorting is used by several schemes proposed later. In 2007, Thodi and Rodriguez [11] exploited histogram shifting technique and prediction error (PE) expansion to improve DE scheme. Applying histogram shifting technique, they eliminate the need for location map and employ information of neighboring pixels to obtain an

efficient PE for expanding. Authors of [11] improve the scheme in [25] especially for higher embedding capacities (EC)s. In 2009, Sachnev *et al.* [4] employed rhombus predictor to embed data into an image. Their scheme divides a cover image into two sets denoted as cross and dot. Half of the data bits are embedded in cross (dot) set and the other half is embedded in dot (cross) set. Their method is better than the one in [25] because they use sorting with regard to local variance, histogram shifting and cross-dot embedding mechanism altogether. Also, the use of rhombus predictor makes sharper error histogram that is an improvement to the scheme of [11].

Modifying the pairs of peak and zero points in the image histogram, Ni *et al.* [3] present an innovative RDH scheme. The pixels between peak and zero points of histogram are modified to make space for embedding data. Lee *et al.* [19] have exploited histogram modification of difference image to embed data. There is a large probability that neighboring pixels in an image have similar pixel values. That means the histogram of differences between two neighboring pixels (*i.e.* the histogram of difference image) is, definitely, sharper than the histogram of the original image. Thus, it provides higher peak point resulting in higher capacity to embed data. It is better to name the scheme in [19] as prediction-error modification, which indicates three operations: predict a pixel, calculate prediction error and modify prediction error to embed data bits. In 2007, Fallahpour and Sedaaghi [26] improved the scheme in [3] by executing it on series of blocks. Almost, all schemes, proposed on the basis of histogram later, use the idea of prediction-error modification. Yang and Tsai [20], later on, introduced a histogram based RDH scheme, in which they used rhombus predictor [4] to embed data. It employs to create prediction-errors which modify to embed data bits. Li *et al.* [21] introduce a RDH scheme based on two-dimensional difference histogram modification and difference-pair-mapping. They use gradient-adjusted-prediction (GAP) predictor to make difference-histogram. The employment of two-dimensional difference-histogram leads to have more embedding capacity

that results in reducing the number of shifted pixels and distortion. Li *et al.* [22], also, propose multiple histograms modification as a new embedding mechanism. They use cross-dot embedding mechanism and rhombus predictor, which are introduced in [4]. Instead of the local variance in [4] and [25], complexity measurement is used in their method to construct prediction-error histogram. Their algorithm has great performance and outperforms the methods in [4], [21]. Ma and Shi [18] propose a RDH algorithm based on code division multiplexing. They employ Walsh Hadamard matrix to generate orthogonal spreading sequences, in which one can embed overlapped data bits without interfering. Like [22], employing cross-dot embedding mechanism and rhombus predictor, their scheme can be considered as a kind of histogram modification that has great performance but not in low EC. In 2017, Wang *et al.* [23] introduced a histogram based method and an organized framework to design multiple RDH scheme with nearly optimal rate and distortion performance. Their scheme is independent of cover images and uses genetic algorithm to realize optimization. In 2019, Xiao *et al.* [24] introduced a content dependent pairwise embedding scheme. In this scheme two-dimensional histogram of prediction-errors is modified to embed data. First, this histogram is divided into specific regions. Then, the expansion bins selection in these regions is formulated as an optimal path searching problem to adaptively modify prediction-errors in order to embed data. They outperform [23].

This paper provides three proposals to improve the efficiency (*i.e.* to decrease the distortion for a specific number of embedding bits) of a RDH method. The first one is a sorting method based on dividing image pixels into cell frequency bands from the lowest to highest one, which range the pixels from smooth to rough. The second proposal is another sorting and concerned with dividing the cell frequency bands into some sub-bands by the use of existence probability of some pixels in cell frequency bands. Employing the two sorting algorithms, one starts embedding from the smoothest pixels towards the roughest and, therefore, the low distortion can be achieved. Hiding intensity analysis, our third proposal is related to adaptive determination of optimum thresholds for a chessboard predictor RDH method in [20] so as to increase the efficiency. The implementation of our proposals and comparing the results with those of the existent RDH algorithms indicate significant improvement in PSNR for a fix number of embedding bits.

2. Related Work

As mentioned, one of the best predictors has ever been presented in RDH schemes is rhombus predictor [4]. It is introduced in [20] as chessboard predictor (CBP) (Fig. 1) as well. In this predictor, black pixels are predicted using white neighbors and vice versa. Let $H_{i,j}$ denotes the intensity of i,j th pixel in a cover image H . Four pixels in the set $\{H_{i-1,j}, H_{i+1,j}, H_{i,j-1}, H_{i,j+1}\}$ form a cell, so as to hide one data bit in $H_{i,j}$. To realize hiding in [20], $H_{i,j}$ can be predicted by its four neighbors as

$$H_{i,j}^p = \lfloor \frac{H_{i,j-1} + H_{i+1,j} + H_{i,j-1} + H_{i,j+1}}{4} \rfloor \quad (1)$$

where $\lfloor \cdot \rfloor$ is the round function. Using $H_{i,j}^p$ and $H_{i,j}$, the prediction error $e_{i,j}$ is computed by

$$e_{i,j} = H_{i,j} - H_{i,j}^p \quad (2)$$

The bit b that can be 0 or 1, changes the error according to two thresholds $SV_p \geq 0$ and $SV_n < 0$ in histogram of the PE. Fig. 2 shows the histogram of PE that has been modified to insert data bits. The serviceable values (SVs) are those, in which the data bits are embedded. Shifting the intensity value of some pixels in two directions, the unserviceable values (USVs) are formed so as to make space and perform hiding. The right shift and left shift involve the increase and decrease of pixel intensities that are at right side of a positive threshold SV_p and at left side of a negative threshold SV_n respectively. The change of error is accomplishing as

$$e'_{i,j} = \begin{cases} e_{i,j} + 1 & \text{if } e_{i,j} > SV_p \\ e_{i,j} - 1 & \text{if } e_{i,j} < SV_n \\ e_{i,j} + \text{sign}(e_{i,j}) b & \text{if } e_{i,j} = SV_p \text{ or } e_{i,j} = SV_n \\ e_{i,j} & \text{else} \end{cases} \quad (3)$$

where sign indicates the signum function. Embedding the data, the intensity of i,j th pixel ($M_{i,j}$) in the marked image M is obtained using (4).

$$M_{i,j} = H_{i,j}^p + e'_{i,j} \quad (4)$$

After transmitting the marked image to a destination, data extraction and cover image reconstruction are done as follows. The recipient computes $e'_{i,j}$ by

$$e'_{i,j} = M_{i,j} - H_{i,j}^p \quad (5)$$

and then retrieves $e_{i,j}$ and extracts bit b using (6).

$$e_{i,j} = \begin{cases} e'_{i,j} - 1 & \text{if } e'_{i,j} > SV_p \\ e'_{i,j} + 1 & \text{if } e'_{i,j} < SV_n \\ e'_{i,j}, b = 0 & \text{if } e'_{i,j} = SV_p \text{ or } e'_{i,j} = SV_n \\ e'_{i,j} - 1, b = 1 & \text{if } e'_{i,j} = SV_p + 1 \\ e'_{i,j} + 1, b = 1 & \text{if } e'_{i,j} = SV_n - 1 \\ e'_{i,j} & \text{else} \end{cases} \quad (6)$$

Finally, the cover image is reconstructed as

$$H_{i,j} = H_{i,j}^p + e_{i,j} \quad (7)$$

It should be noted that $H_{i,j}^p$ can be computed at destination from $\{M_{i-1,j}, M_{i+1,j}, M_{i,j-1}, M_{i,j+1}\}$ using (1), in which H is replaced by M . The CBP in [20] can be started from the prediction for either black or white pixels. Starting from the use of black pixels for the prediction, data is embedded in the

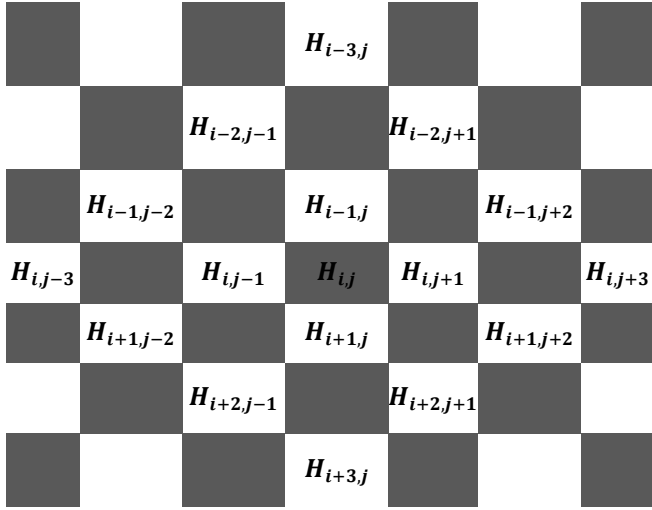


Fig. 1. A part of an image, whose pixels are divided into white and black sections.

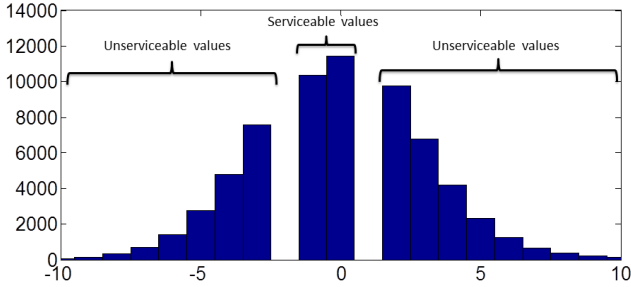


Fig. 2. Serviceable and unserviceable values in the histogram of prediction errors.

errors using (1) for the white pixels. After embedding a number of data bits in the white pixels, embedding continues on black ones by the prediction that is calculated from four neighboring white pixels, and this process can be iterated to embed all data bits.

3. PROPOSED SCHEME

Our proposal comprises the introduction of two new sorting methods and the adaptive determination of the thresholds (SV_p, SV_n) in the embedding method described in Section 2. They are introduced and explained as follows.

3.1. Sorting Using Cell Frequency Spectrum

On basis of local complexity, image pixels in [6] are divided into smooth and rough groups and the bits are hidden in smooth and rough regions in an adaptive manner. Also in [22], some thresholds are exploited to distinguish smooth image regions from rough ones. In this paper, to distinguish image regions, we define cell frequency bands, which are ranged from ultra-low cell frequency (ULCF) to ultra-high cell frequency (UHCF) bands. In the following, this ranging is explained.

As explained in Section 2, a cell comprises 4 pixels that are neighbor to a target pixel. Data bits are embedded in target pixels and neighboring ones remain intact. We determine cell smoothness or cell roughness using local difference (LD) of the neighboring pixels, and then classify cells to different cell frequency bands. For the target pixel $H_{i,j}$ in Fig. 1, neighboring white pixels $H_{center} =$

$\{H_{i-1,j}, H_{i+1,j}, H_{i,j-1}, H_{i,j+1}\}$ is sorted from small to large intensity and the sorted set is denoted as $\{S1, S2, S3, S4\}$. In order to classify a cell, a parameter named LD_{center} is computed according to (8).

$$LD_{center} = (|S4 - S3| + |S4 - S2| + |S4 - S1| + |S3 - S2| + |S3 - S1| + |S2 - S1|)/6 \quad (8)$$

Because we know $S4 > S3 > S2 > S1$, (8) can be simplified to

$$LD_{center} = (S4 - S1)/2 + (S3 - S2)/6 \quad (9)$$

Equation (9) shows the allocation of more weight to the difference of side pixels ($S4 - S1$) than middle ones ($S3 - S2$). Neighboring side cells ($H_{left}, H_{right}, H_{low}, H_{high}$) in addition to H_{center} is also exploited to determine the smooth or the rough region of the image. The side cells include three pixels instead of four pixels, *i.e.* $H_{right} = \{H_{i+1,j+2}, H_{i,j+1}, H_{i-1,j+2}\}$, $H_{left} = \{H_{i,j-1}, H_{i+1,j-2}, H_{i-1,j-2}\}$, $H_{high} = \{H_{i-2,j-1}, H_{i-1,j}, H_{i-2,j+1}\}$ and $H_{low} = \{H_{i+2,j-1}, H_{i+1,j}, H_{i+2,j+1}\}$. If three pixels in the side cells are sorted from small to large intensity and their rearrangement is called $\{I1, I2, I3\}$, we can compute LD for the side cells as

$$LD_{side} = (|I3 - I2| + |I3 - I1| + |I2 - I1|)/3 = 2(I3 - I1)/3 \quad (10)$$

The quantity LD for all four side cells are calculated using (10) and are denoted as $LD_{right}, LD_{left}, LD_{high}$ and LD_{low} . The cell frequency classification is accomplished according to the following mean value of the local differences

$$f_c = \overline{LD} = (LD_{center} + LD_{right} + LD_{left} + LD_{high} + LD_{low})/5 \quad (11)$$

In Table 1, regarding f_c and the thresholds $T_{ulcf}, T_{vlcf}, T_{lcf}, T_{mcf}, T_{hcf}$ and T_{vhcf} , the cells can be classified to ultra-low cell frequency (ULCF), very low cell frequency (VLCF), low cell frequency (LCF), medium cell frequency (MCF), high cell frequency (HCF), very high cell frequency (VHCF) and ultra-high cell frequency (UHCF). The bands with lower cell frequency are more desirable and make less distortion for data embedding. Therefore, the data is embedded in a cover image according to the sorting of Table 1.

TABLE 1 Cell frequency spectrum

Thresholds	Cell Band
$f_c < T_{ulcf}$	ULCF
$T_{ulcf} < f_c \leq T_{vlcf}$	VLCF
$T_{vlcf} < f_c \leq T_{lcf}$	LCF
$T_{lcf} < f_c \leq T_{mcf}$	MCF
$T_{mcf} < f_c \leq T_{hcf}$	HCF
$T_{hcf} < f_c \leq T_{vhcf}$	VHCF
$T_{vhcf} < f_c$	UHCF

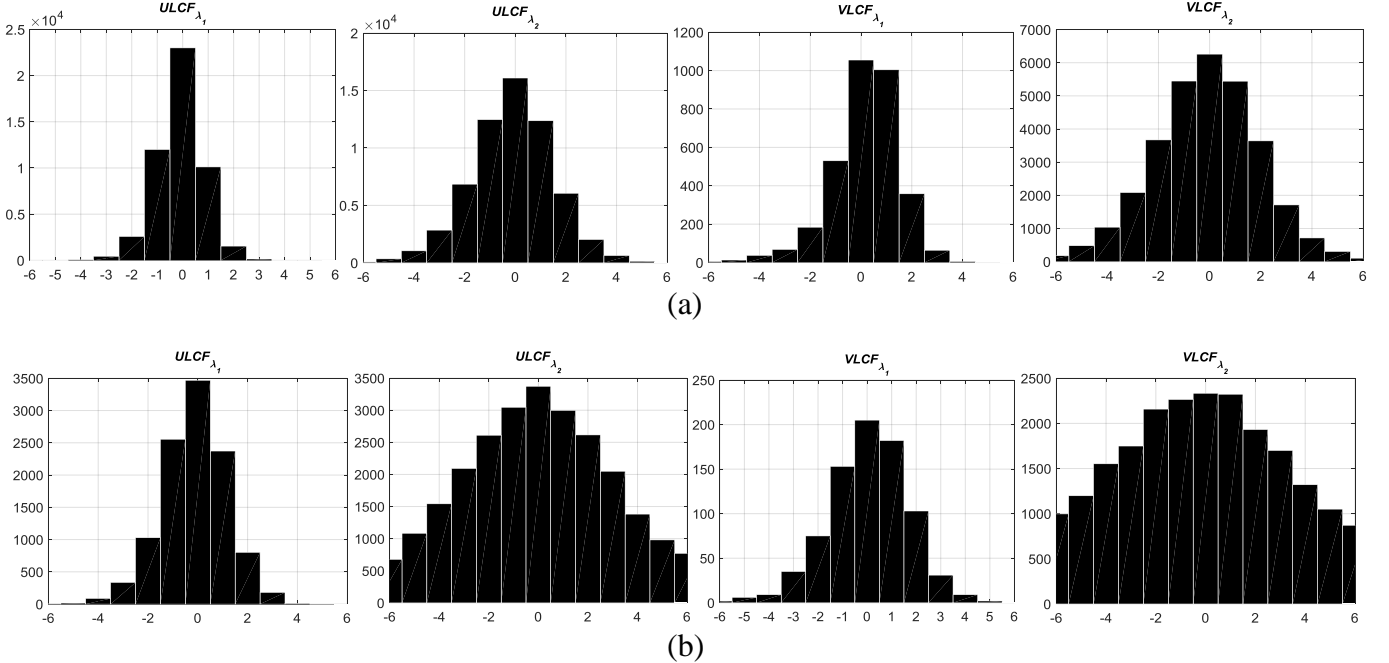


Fig. 3. Prediction errors histogram of two different images (a) F16 and (b) Lake in two different sub-bands of ULCF and VLCF bands respectively ($ULCF_{\lambda_1}$ and $ULCF_{\lambda_2}$) and ($VLCF_{\lambda_1}$ and $VLCF_{\lambda_2}$) sub-bands.

3.2. Sorting Based on Pixel Existence Probability (SPEP)

The ULCF band, for its sharper histogram of PE, is the best band for data embedding. This subsection describes another sorting, in which the existence probability of pixels in a part of ULCF band with lower LD, denoted partial ULCF, is employed to divide each band to some sub-bands.

ULCF band with lower LD, denoted partial ULCF, is employed to divide each band to some sub-bands. In this section, our explanation is focused on the procedure for sub-banding ULCF band. Obviously, the same procedure can be utilized for the other cell frequency bands. Let \tilde{X}_i indicates the set of pixels among white pixels with intensity x_i and take \tilde{X}_i^p the set of pixels with the same intensity that belongs to partial ULCF. In addition, let $h(x_i)$ and $h_p(x_i)$ show the number of pixels in \tilde{X}_i and \tilde{X}_i^p respectively. Because we have $\tilde{X}_i^p \subset \tilde{X}_i$, if a pixel p_i is selected randomly from \tilde{X}_i , the probability that this pixel being in \tilde{X}_i^p is obtained from (12).

$$f_{x_i} = P(p_i \in \tilde{X}_i^p | p_i \in \tilde{X}_i) = \frac{h_p(x_i)}{h(x_i)} \quad (12)$$

f_{x_i} is called the existence probability of pixel p_i in partial ULCF and it is calculated according to (12) for $x_i = 0$ to 255. Considering all of obtained values are $F = \{f_{x_0}, \dots, f_{x_i}, \dots, f_{x_{255}}\}$, $x_{m_1} = \arg \max_{0 \leq i \leq 255} (f_{x_i})$ is the pixel intensity, on which data embedding has the least distortion. That is because the maximum, $f_{x_{m_1}}$, indicates the probability of a pixel being in partial ULCF with intensity x_{m_1} is maximum. Therefore, the higher probability of x_{m_1} in partial ULCF, that is the smoothest part of the image, determines that x_{m_1} is the smoothest pixel. The conclusion is that embedding data in pixels set with intensity x_{m_1} introduces less distortion

than others. Reasoning in a same way, the embedding should be continued with pixels having the intensity $x_{m_2} = \arg \max_{0 \leq i \leq 255} (f_{x_i})$ and so forth.

To implement the aforementioned procedure efficiently in ULCF band, *i.e.* dividing this band into several sub-bands, we arrange the members of set F from large to small, and denote it as $F_S = \{f_{s_0}, \dots, f_{s_i}, \dots, f_{s_{255}}\}$. The set $\tilde{X}_S^{ulcf} = \{\tilde{X}_{s_0}^{ulcf}, \tilde{X}_{s_1}^{ulcf}, \dots, \tilde{X}_{s_{255}}^{ulcf}\}$ shows the pixel sets in ULCF band corresponding to F_S . It is noted that $\tilde{X}_{s_i}^{ulcf}$ is itself a set containing the pixels with intensity x_{s_i} . Set $\tilde{X}_{s_0}^{ulcf}$ is the smoothest and $\tilde{X}_{s_{255}}^{ulcf}$ is the roughest and data hiding is accomplished from $\tilde{X}_{s_0}^{ulcf}$ to $\tilde{X}_{s_{255}}^{ulcf}$. In order to reduce the complexity of implementation, we can divide \tilde{X}_S^{ulcf} into some classes and perform data hiding for each class. We classify \tilde{X}_S^{ulcf} as $\tilde{X}_S^{ulcf} = \{ULCF_{\lambda_1}, ULCF_{\lambda_2}, \dots, ULCF_{\lambda_m}\}$, ($m < 5$). It is divided into m classes with $ULCF_{\lambda_1} = \{\tilde{X}_{s_0}^{ulcf}, \tilde{X}_{s_1}^{ulcf}, \tilde{X}_{s_2}^{ulcf}, \dots, \tilde{X}_{s_a}^{ulcf}\}$ so that $f_{s_i} > f_{s_a}$ for each $i < a$, $ULCF_{\lambda_2} = \{\tilde{X}_{s_{a+1}}^{ulcf}, \tilde{X}_{s_{a+2}}^{ulcf}, \tilde{X}_{s_{a+3}}^{ulcf}, \dots, \tilde{X}_{s_b}^{ulcf}\}$ so that $f_{s_j} > f_{s_b}$ for each $a < j < b$ and so forth. Starting data hiding from $ULCF_{\lambda_1}$ to $ULCF_{\lambda_m}$, we can reduce the complexity of implementation with loss of some degree of quality for the marked image in comparison with using $\{\tilde{X}_{s_0}^{ulcf}, \tilde{X}_{s_1}^{ulcf}, \dots, \tilde{X}_{s_{255}}^{ulcf}\}$. The classification can be viewed as the split of ULCF band into m sub-bands. For example, if there are two classes, we separate ULCF into two smoother $ULCF_{\lambda_1}$ and rougher $ULCF_{\lambda_2}$ sub-bands. $ULCF_{\lambda_1}$ and $ULCF_{\lambda_2}$ present the pixels in ULCF band that are respectively more and less predictable. Using this information we can divide other bands, *e.g.* VLCF band, to different sub-bands. Although we can use this procedure to divide all bands to

TABLE 2 Hiding intensity analysis

(a)						(b)					
Number	SV	N_{SV}	N_{USV}	HI	PoH	Number	SV	N_{SV}	N_{USV}	HI_{sorted}	
1	0,-1	21795	43819	0.49	15371	1	4,-5	3734	4214	0.89	
2	1,-2	17384	26435	0.66	14097	2	3,-4	6963	7948	0.88	
3	2,-3	11524	14911	0.77	10131	3	2,-3	11524	14911	0.77	
4	3,-4	6963	7948	0.88	6517	4	1,-2	17384	26435	0.66	
5	4,-5	3734	4214	0.89	3515	5	0,-1	21795	43819	0.49	

different sub-bands, it is more efficient applying this just for ULCF and VLCF bands. This is a trade-off between computational complexity and marked image quality. In the following, we illustrated this method using an example.

Fig. 3 shows simulation of PEs histogram of F16 and Lake images, that is calculated for two different sub-bands in ULCF and VLCF bands respectively ($ULCF_{\lambda_1}$ and $ULCF_{\lambda_2}$) and ($VLCF_{\lambda_1}$ and $VLCF_{\lambda_2}$). In this simulation, 3000 pixels of ULCF band, which have lower LD are chosen to use as partial ULCF and the same is applied to VLCF band so as to divide it into two different sub-bands. These sub-bands are classified according to $F_S = \{f_{s_0} = 0.37, f_{s_a} = 0.01\}$ and $F_S = \{f_{s_0} = 0.33, f_{s_a} = 0.05\}$ respectively for F16 and Lake. For F16 with $f_{s_a} = 0.01$, the pixels with intensity in interval $210 < x_i < 225$ have $f_{x_i} > 0.01$. Choosing these pixels in ULCF and VLCF bands, we form respectively $ULCF_{\lambda_1}$ and $VLCF_{\lambda_1}$ sub-bands and subsequently choosing other pixels in these bands, we construct $ULCF_{\lambda_2}$ and $VLCF_{\lambda_2}$ (Fig. 3a). Accordingly, for Lake by choosing $f_{s_a} = 0.05$, the pixels with intensity in interval $220 < x_i < 231$ are used to construct these sub-bands (Fig. 3b).

As it is demonstrated, for both images the PEs belong to $ULCF_{\lambda_1}$ sub-band has sharper histogram that means these pixels are smoother and more predictable than $ULCF_{\lambda_2}$ ones. Also, $VLCF_{\lambda_1}$ provides sharper PEs histogram than $VLCF_{\lambda_2}$. It concludes that $ULCF_{\lambda_1}$ and $VLCF_{\lambda_1}$ are more eligible to embed data bits than $ULCF_{\lambda_2}$ and $VLCF_{\lambda_2}$ respectively.

In practice, in implementation of SPEP method, (1) is employed to obtain the predicted intensity of the pixels that can be used instead of the pixel own intensities.

3.3. Hiding Intensity Analysis

In this section, we introduce hiding intensity analysis (HIA) that determines adaptively two thresholds $SV_p \geq 0$ and $SV_n < 0$ in CBP method [20] to improve the efficiency in data embedding with low distortion. As explained in Section 2, the serviceable and unserviceable values are to be specified according to two thresholds SV_p and SV_n . The thresholds can be $(SV_p, SV_n) = (0, -1)$ or $(1, -2)$ or etc. The number of serviceable values (N_{sv}) and unserviceable ones (N_{usv}) depends on the pair (SV_p, SV_n) . N_{usv} is the number of pixels distorted to make space for embedding bits. Therefore, if N_{usv} is kept minimum for a specified number of embedding bits (N_b), the distortion for the marked image will be less. In this regard, we define a hiding intensity (HI) criteria that is a function of (SV_p, SV_n) and given by

Algorithm 1: Adaptive determination of SV = (SV_p, SV_n) according to HIA

```

Do
  if  $N_b > N_{sv}(k_{poh})$  then
     $SV(k_{poh})$  is exploited
     $N_b = N_b - N_{sv}(k_{poh})$ 
    go to next band, sub-band or step
  else
    for  $k = 1:K$ 
      if  $N_b/N_{USV} \leq HI_{sorted}(k)$  then
         $SV(k)$  is exploited
         $N_b = 0$ 
        Break For Loop
      end if
    end for
  end if
  while  $N_b > 0$ 

```

$$HI(SV_p, SV_p) = N_{sv}/N_{usv} \quad (13)$$

The HI criteria shows how many bits can be embedded for each unserviceable pixels. Table 2(a) lists the aforementioned parameters of a sample image for different (SV_p, SV_n) .

Our above justification is, therefore, concluded in a procedure that we start embedding bits with the pair (SV_p, SV_n) , for which $HI(SV_p, SV_p)$ is maximum. However, if the number of hiding bits N_b is more than the number of serviceable values (N_{sv}) corresponding to the maximum HI , it is required to reiterate the CBP procedure. For example, hiding bits in a cell frequency band, it is required to continue hiding the rest of bits in higher one because N_{sv} corresponding to the maximum HI is less than N_b . This can distort more the marked image than we start with (SV_p, SV_n) , for which $N_{sv} \geq N_b$ or for which $N_{sv} = N_{sv}^{Max}$ in case the condition $N_{sv} \geq N_b$ cannot be satisfied for any (SV_p, SV_n) . It is noted that N_{sv}^{Max} is the maximum number of serviceable values obtained for a specific (SV_p, SV_n) , e.g. $N_{sv}^{Max} = 21795$ for $(SV_p = 0, SV_n = -1)$ in Table 2(a).

As a result, we introduce another criteria called power of hiding (PoH) and defined as

$$PoH = N_{sv} \times HI = N_{sv}^2/N_{USV} \quad (14)$$

The criteria PoH is a compromise that emphasizes both N_{sv} and HI , and its maximum is used to develop our procedure for adaptive determination of $SV = (SV_p, SV_n)$. In order to describe the procedure, let us sort the rows of Table 2(a) according to HI values from high to low and put the results in Table 2(b).

Also, let us obtain the row number corresponding to the maximum PoH as

$$k_{poh} = \arg \max_{1 \leq k \leq K} PoH(k) \quad (15)$$

where the capital K indicates the total number of rows. For example, $k_{poh} = 5$ and $\max PoH = PoH(5) = 15371$ in Table 2(b). Now, the procedure to determine adaptively $SV = (SV_p, SV_n)$ for embedding bits is given by Algorithm 1.

3.4. Overflow and Underflow

It is possible for a marked image to have some pixels that get overflow or underflow in grayscale values, meaning that the grayscale values of some pixels in the marked image may exceed the upper bound (255 for an eight-bit grayscale image) or lessen the lower bound (“0”), respectively.

In [5], Luo *et al.* propose a useful method to overcome overflow or underflow (OU). In [5], after a level of data hiding, if there are 256 and -1, they will be modified to 255 and 0. In order to avoid overlapping with original ones, they assign 1 to all modified pixels (*i.e.* modified 256 and -1 to 255 and 0) and 0 to the original ones. These 0 and 1 as overhead information are compressed and sent with the marked image. At the receiver using overhead information, modified pixels will be recovered.

In this section, a novel algorithm is proposed to decrease or eliminate this need for overhead information in [5]. First of all, let's define three pixels group, green (C_g), yellow (C_y) and red (C_r) pixels. C_g is a pixel with no or very low probability of OU. C_y is susceptible to OU, and C_r is the pixel in which OU is occurred. Embedding is done on green pixels (C_g s), and C_y s are ignored in the process of embedding because they have more possibility to make C_r s. Also, after data embedding C_r s must be managed.

Algorithm 2: Classify pixels to C_y or C_g

```

if  $|255 - H_{i,j}^p| < \tau_2$  and  $H_{i,j} \geq H_{i,j}^p$  then
     $H_{i,j}$  is a  $C_y$ 
else if  $|H_{i,j}^p| < \tau_1$  and  $H_{i,j} < H_{i,j}^p$  then
     $H_{i,j}$  is a  $C_y$ 
else
     $H_{i,j}$  is a  $C_g$ 
end if

```

Classify a pixel to C_y or C_g is done using Algorithm 2, where τ_1 and τ_2 are positive integer that are exploited to classify some pixels maybe near lower bound or upper bound to C_y . Also, in this algorithm, $H_{i,j}^p$ is the prediction amount of $H_{i,j}$. It is calculated using (1). The greater τ_1 and τ_2 is selected, the more pixels are classified as C_y . It leads to less probability of happening C_r .

With an example (Fig. 4), we will explain Algorithm 2. Let's choose $\tau_1 = 2$ and $\tau_2 = 2$. Regarding to Algorithm 2 for Fig. 4a, we have $|255 - H_{i,j}^p| < \tau_2$ but not $H_{i,j} \geq H_{i,j}^p$ ($H_{i,j}^p = 254$, $H_{i,j} = 253$); Therefore, it will be classified as C_g . In this figure regarding $H_{i,j} < H_{i,j}^p$, after embedding data, $H_{i,j}$ either remains intact or decreases so it never overflows. There is a similar argument for Fig. 4b. In this cell, we have $|H_{i,j}^p| < \tau_1$ but not $H_{i,j} < H_{i,j}^p$ ($H_{i,j}^p = 0$, $H_{i,j} = 1$); so $H_{i,j}$ either remains intact or increases. Therefore, it never gets underflow and is also considered as a C_g .

In Fig. 4c, considering $H_{i,j} > H_{i,j}^p$ ($H_{i,j}^p = 254$, $H_{i,j} = 255$), there is considerable possibility that $H_{i,j}$ overflows by embedding data. Therefore, this pixel is classified as C_y and will be ignored in the process of embedding.

Happening OU in C_g s is not impossible. In some pixels, there is maybe more variance between $H_{i,j}$ and $H_{i,j}^p$ making more probability of OU and producing C_r . By choosing proper τ_1 or τ_2 especially in higher cell frequency bands, it may prevent producing C_r . However, one can manage OU after embedding data by using method presented in [5].

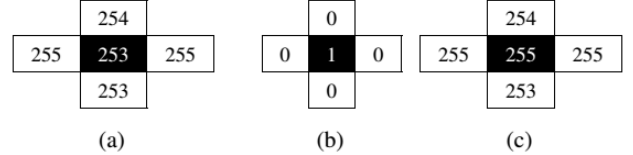


Fig. 4. Classify three pixels, were centred on three different cells, to green pixel (C_g) or yellow one (C_y). The 253 and 1 are classified as green pixels, and 255 as a yellow one.

4. Whole Proposed RDH

In this section, the methods of data embedding, data extracting and retrieving the cover image are described as a whole. To embed data, the total image pixels are divided into two black and white pixel groups. Also, all bits of the data are divided into two equal parts of the black and the white ones to be respectively embedded in the black and white pixels. Let's call data bits to be embedded in white (or black) pixels as white (or black) data. Embedding data can be begun with white or black ones. If data is embedded in the white pixels, black ones remain unchanged. As the next step, in the same way, data is embedded in the black pixels and white ones remain intact. We define the whole embedding in white or black pixels as one embedding level.

After the end of hiding process, overhead information, such as beginning from the white or black pixels, the total number of data bits, SV values, the number of data hiding steps, and OU information, is embedded in the determined locations of the image, *e.g.* in the first or last row (or column) of the image that has been remained intact during data embedding.

The process of hiding, starting with black pixels is projected as follows.

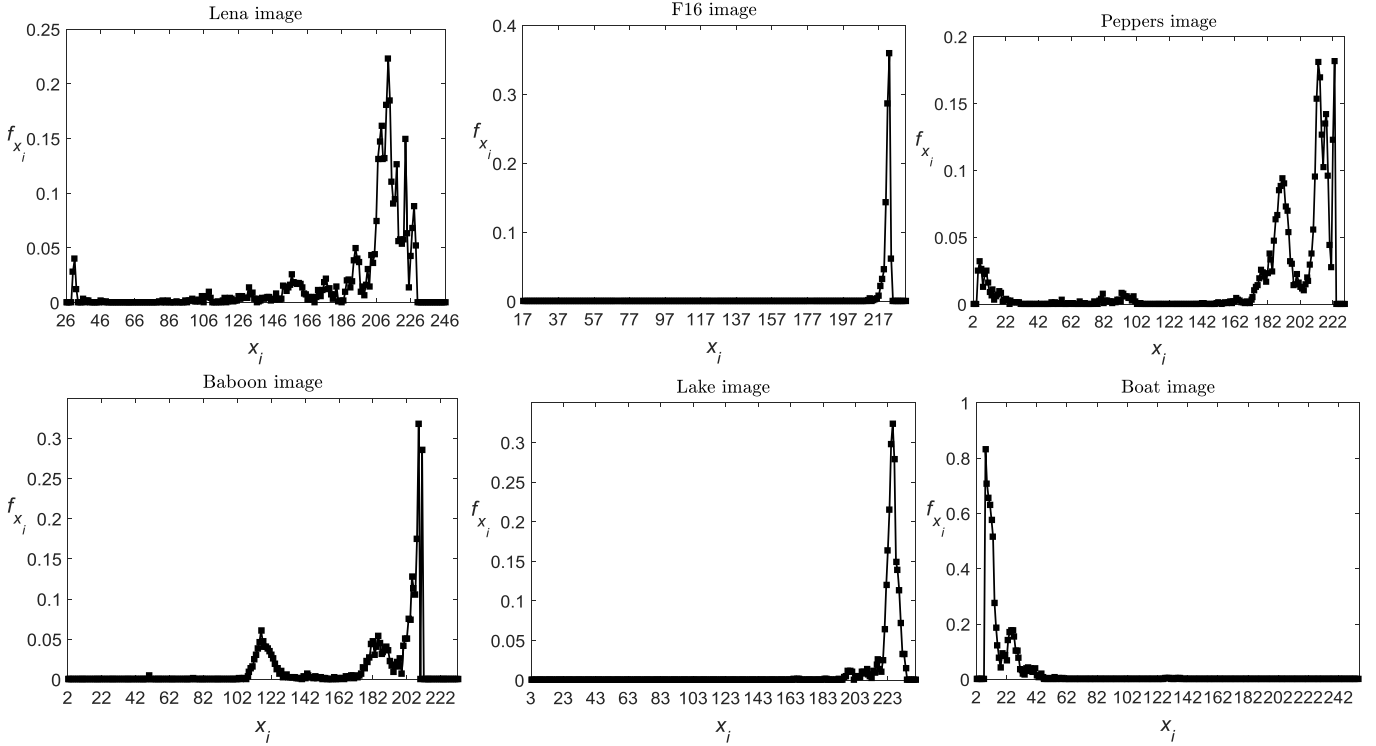


Fig. 5. Calculate f_{x_i} for pixel group with x_i intensity in test images.

- 1) Calculate f_c for each cell. Cells are classified according to the f_c (Table 1) (ULCF as the first band and UHCF as the last one)). Divide ULCF and VLCF bands into several sub-bands according to Section 3.1. Embedding is begun with $ULCF_{\lambda_1}$.
- 2) Considering a cell, using (1), $H_{i,j}^p$ is predicted. Prediction errors ($e_{i,j}$) in the selected frequency band or sub-band are calculated for whole cells using (2). They have been sorted corresponding to their f_c . In these equations, (i,j) are the rows and columns of the black pixels in the selected frequency band or sub-band.
- 3) According to Section 3.3, for different SV values, HI and PoH are calculated; the best SV (SV_n, SV_p) will be picked up according to the number of data bits.
- 4) Calculate $e'_{i,j}$ according to (3). In this equation, we apply SV just for C_g s to control overhead information for OU (Section 3.4).
- 5) Marked image is created using (4). If all black data bits are embedded, we keep on hiding in white pixels (*i.e.* white data) with start from step 1. Otherwise, we continue embedding in black data for the higher cell frequency bands starting from step 2. Also, after one embedding level, it will be continued to more levels to embed whole data. After any embedding level we must check for C_r . If there is C_r , we can use method that is presented in [5] to manage it.
- 6) Finally, overhead information is embedded in the marked image.

At the receiver, initially, the overhead information is extracted. Based on the number of data bits and hiding steps,

starting from the black or white pixels and needed information of OU, data extraction and original image retrieving are begun. Regarding that hiding process has been established by starting from black cells, extracting data bits and retrieving of the cover image must be started from white ones explained as follows.

- 1) Classification of cells is done using neighboring pixels according to the calculation of f_c . Select ULCF as the first band and UHCF as the last one. Divide ULCF and VLCF bands into several sub-bands. Sort cells based on f_c .
- 2) $H_{i,j}^p$ is computed at destination from $\{M_{i-1,j}, M_{i+1,j}, M_{i,j-1}, M_{i,j+1}\}$ using (1), in which H is replaced with M . Then using (5), $e'_{i,j}$ is calculated ((i,j) are the rows and columns of the white pixels in these equations).
- 3) Using (6), $e_{i,j}$ is recovered for C_g s. It should be noted that (SV_n, SV_p) has been sent to the recipient as overhead information.
- 4) A pixel coordinate (i,j) of the original image is retrieved for the specified cell frequency band, using (7). It continues for whole white pixels.
- 5) If all white data bits are extracted, we continue to extract black data using neighboring white pixels starts from Step 1. Otherwise, we will keep on extracting in the higher cell frequency bands or sub-bands starting from step 2. If we are in the largest one UHCF, we would go to next level of extraction beginning with ULCF sub-bands in order to extract more bits and restore the original image.

TABLE 3 PSNR results for two f_c s in different ECs for test images

	EC	0.5	1	2	5	10	20	40	70	100	$\times 10^3$ bits
Lena	$f_c = \overline{LD}$	74.51	71.04	67.43	62.78	59.27	55.81	52.23	48.59	45.63	dB
	$f_c = LD_{center}$	72.50	69.50	66.42	62	58.63	55.34	52.03	48.41	45.53	dB
F16	$f_c = \overline{LD}$	77.04	73.94	70.84	66.45	63.11	59.62	55.84	52.43	49.44	dB
	$f_c = LD_{center}$	75	72.72	69.53	65.20	62.36	58.88	55.31	52.27	49.25	dB
Peppers	$f_c = \overline{LD}$	69.98	66.61	63.45	59.18	55.91	52.55	48.66	43.75	40.58	dB
	$f_c = LD_{center}$	69.13	66.12	63	58.72	55.41	52.31	48.54	43.64	40.46	dB
Baboon	$f_c = \overline{LD}$	69.43	66.27	62.93	58.47	54.93	50.18	44.33	39.01	30.13	dB
	$f_c = LD_{center}$	68.52	65.24	62.13	57.89	54.55	49.89	44.06	38.81	30.65	dB
Lake	$f_c = \overline{LD}$	74.17	71	67.67	62.47	58.10	53.23	48.47	43.02	39.44	dB
	$f_c = LD_{center}$	72.47	69.51	66.02	61.19	57.35	53.09	48.16	42.92	39.35	dB
Boat	$f_c = \overline{LD}$	73.02	69.66	66.16	61.26	57.09	52.88	48.82	43.79	40.50	dB
	$f_c = LD_{center}$	70.96	67.70	64.52	60.15	56.58	52.88	48.58	43.69	40.47	dB

TABLE 4 The effect of HIA and SPEP tools to improve marked image quality of test images

	EC	0.5	1	2	5	10	20	40	70	100	$\times 10^3$ bits
Lena	HIA	74.66	71.42	68.43	64.10	60.60	56.94	52.97	48.88	45.73	dB
	SPEP	74.65	71.35	68.14	63.86	59.63	55.82	52.24	48.62	45.63	dB
	SPEP & HIA	76.42	73.05	69.56	64.47	61	56.93	53.09	48.92	45.74	dB
F16	HIA	76.35	73.16	70.05	66.33	62.70	59.96	55.84	52.67	49.91	dB
	SPEP	77.62	73.95	70.85	66.63	63.32	59.94	55.85	52.43	49.45	dB
	SPEP & HIA	77.62	74.65	71.64	67.54	64.21	59.96	56.53	52.97	50.03	dB
Peppers	HIA	73.14	70.17	66.83	61.71	58.04	54.28	49.65	44.57	41.14	dB
	SPEP	70.26	66.87	63.57	59.30	55.99	52.54	48.69	43.79	40.59	dB
	SPEP & HIA	74.69	70.80	66.87	62.03	58.15	54.35	49.66	44.61	41.18	dB
Baboon	HIA	71.59	68	64.56	59.85	56.10	50.95	44.59	39.29	35	dB
	SPEP	69.46	66.34	62.94	58.49	54.94	50.18	44.34	39.17	30.14	dB
	SPEP & HIA	71.42	68.06	64.85	60.05	56.06	50.95	44.61	39.32	35	dB
Lake	HIA	72.65	69.35	65.77	62.22	58.10	53.80	48.93	43.45	39.80	dB
	SPEP	74.52	71.43	68.32	63.90	58.19	53.22	48.51	43.02	39.44	dB
	SPEP & HIA	76.72	73.54	69.83	63.86	58.82	53.64	49.1	43.45	39.80	dB
Boat	HIA	73.18	69.73	66.83	61.59	57.74	53.78	49.31	44.29	40.83	dB
	SPEP	73.13	70.01	66.69	61.53	57.24	52.88	48.88	43.79	40.51	dB
	SPEP & HIA	75.67	71.90	68.01	62.37	58.36	53.87	49.31	44.32	40.88	dB

5. Experimental Result

We have conducted several experiments to certify the performance of the proposed method in hiding capacity and image quality of a marked image. Six gray scale images, Lena, F16, Peppers, Baboon, Lake, and Boat all 512×512 in size are used as test images. We embed pseudo-random binary data in the test images. PSNR is exploited to be a measure of marked image quality in these experiments. According to thresholds $T_{ulcf} = 3.3$, $T_{vlcf} = 4.5$, $T_{lcf} = 6$, $T_{mcf} = 9$, $T_{hcf} = 13$, and $T_{vhcf} = 18$, cells are divided into ULCF, VLCF, LCF, MCF, HCF, VHCF and UHCF bands

(Table 1). In this simulation, UHCF band that involves roughest cells is ignored. As stated before, if hiding is initially executed with white pixels, black ones as neighboring pixels will be remained intact. Hence, the next step of embedding is begun with black ones, while all the thresholds are added to a small bias around 0.3 to separate cell frequency bands. This bias account for the reduction of image smoothness after one embedding step.

In the Lena and F16, because of having no pixel near the upper or lower bound, the OU may just be occurred in higher EC. In Peppers, Baboon, and Lake the underflow is more possible due to the presence of pixels near lower bound while in boat they exist near both lower and upper bounds. Liable

pixels to underflow are put in the borders of the Lake image, *e.g.* pixels in row 512, that are not used to embed data bits in our implementation. Also in Boat, pixels exposed to underflow or overflow keep in UHCF band that ignores in data hiding process. There is no underflow in $EC = 10^5$ bits for Peppers (.res) and Baboon by choosing $\tau_1 = 13$ (.res) and $\tau_1 = 37$ in Algorithm 2 and so ignoring 2470 (.res) and 959 pixels, or cells, of these two images, *i.e.* these pixels will be considered as \mathcal{C}_y .

In this simulation, the ULCF and VLCF bands are employed and are divided into two different sub-bands. Fig. 5 shows probability f_{x_i} for pixels with x_i intensity in test images. We use 3000 pixels of ULCF band with lower LD as partial ULCF. According to this figure and choosing $f_{s_a} = 0.04, 0.01, 0.03, 0.05, 0.05$ and 0.02 respectively for Lena, F16, Peppers, Baboon, Lake and Boat, we divide ULCF and VLCF bands into two sub-bands. In this way, with respect to picked f_{s_a} values, approximately the pixels with intensities $202 < x_i < 229$, $210 < x_i < 225$, $183 < x_i < 223$, $196 < x_i < 212$, $220 < x_i < 231$, and $7 < x_i < 39$ are chosen in ULCF or VLCF as $ULCF_{\lambda_1}$ or $VLCF_{\lambda_1}$ sub-bands respectively for Lena, F16, Peppers, Baboon, Lake and Boat. Other pixels in ULCF or VLCF can, therefore, be selected respectively as $ULCF_{\lambda_2}$ or $VLCF_{\lambda_2}$.

In order to demonstrate the importance of choosing $f_c = \overline{LD}$ as in (11), we provide the results of PSNR in different ECs for setting $f_c = LD_{center}$ ((9)) and $f_c = \overline{LD}$ for test images. The calculated PSNR is listed in Table 3, where the role of side cells to improve marked image quality in specified ECs is not unassailable. This improvement is more significant in low ECs. Also, this improvement on smoother images, such as F16, is more considerable than rougher ones, like Baboon.

For example in F16, in $EC = 0.5 \times 10^3$ bits, we achieve more than 2 dB improvement in marked image quality using side cells along with center one. In the review of the Lena image as a middle one in the term of roughness or smoothness, the improvement respectively is more than 1.5 dB and 0.7 dB for $EC = 1 \times 10^3$ and $EC = 5 \times 10^3$ bits.

Table 4 demonstrates that the HIA and SPEP tools improve quality of the marked image in test images. The comparison of results for $f_c = \overline{LD}$ in Table 3 and HIA and SPEP in Table 4 reveals that they are more effective to improve marked image quality in lower ECs. However, in general kind of view, the effect of SPEP to improve marked image quality is more significant than HIA in the smoother images. In other words, the HIA's is more effective than SPEP to improve PSNR in rougher images. For example, in ECs less than 20×10^3 (Table 4), there is no positive effect in using HIA for F16 and Lake while for Baboon in these ECs, the HIA improves quality of the marked image, at least 1dB. This improvement for the Peppers is more than 2 dB, *i.e.* HIA effect on PSNR, that is listed in Table 4, is compared with results for $f_c = \overline{LD}$ in Table 3. In the Boat and Lena, the impact of HIA rather than SPEP or vice versa is not significantly different in most ECs. However, using HIA in company with SPEP, one can observe from Table 4 that the PSNR improvement is noticeable. For example, in Boat, for $EC = 10^4$ bits, the use of SPEP and HIA together achieves

1.12 dB and 0.62 dB enhancement, respectively, over the use of SPEP and HIA individually. This improvement in most cases is more than when HIA and SPEP are individually employed.

In the Fig. 6, a comparison between the proposed scheme and the schemes in [4], [21], [23] is performed for test images. In our scheme, we use HIA with two novel sorting methods that are sorting by splitting image into cell frequency bands and another sorting SPEP. It can be seen that the image quality of the marked image is significantly improved, especially in lower ECs. Comparing with [4], the improvement for the proposed scheme in some ECs is even more than 3 dB. Fig. 6 illustrates the separation of image pixels into the cell frequency bands together with the separation of the two lowest band, ULCF and VLCF, into two different sub-bands have led to the identification of the most suitable pixels, which make less distortion especially in lower ECs. Also, using the HIA, the optimal prediction error is chosen to achieve minimum distortion of the marked image.

Reference [21] proposes a RDH scheme based on two-dimensional difference histogram modification and difference-pair-mapping (DPM). This scheme provides a good improvement in the marked image quality, especially in low ECs. In [21], the slope of the PSNR reduction is more than our and other considered schemes. The proposed algorithm presents superior results to the scheme in [21], especially in higher ECs. The slope of the PSNR reduction for the scheme of [23] is approximately the same as ours. The improvement over this scheme, for whole test images, is quite tangible. In lower ECs, [21] and [23] schemes improve the [4] ones.

6. Conclusion

We propose two novel sorting methods in order to classify cells into different cell frequency bands and divide a cell frequency band into different sub-bands. In this way, smooth pixels are better identified and more predictability for data hiding is achieved. Also, we propose a hiding intensity analysis (HIA) so as to produce optimal PE that in turn, makes less distortion to the marked image. The comparison of the proposed scheme with other state of the art schemes confirms that our scheme improves significantly the image quality of the marked image, especially for lower ECs. The presented tools in this paper, the separation to different cell frequency bands, SPEP and HIA, may also be exploited for other areas of data hiding.

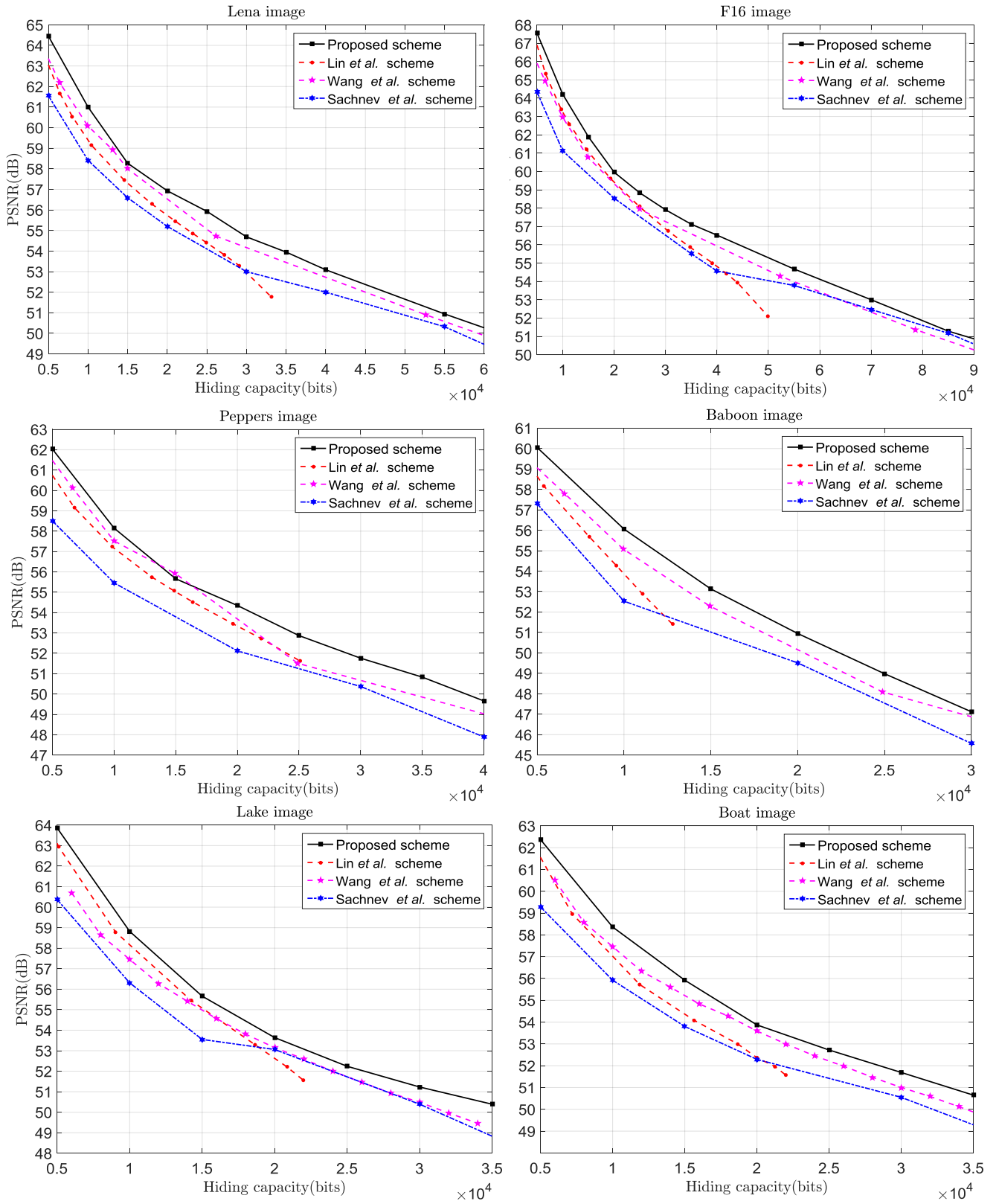


Fig. 6. Comparing the performance of the proposed scheme and Lin et al. [21], Wang et al. [23], and Sachnev et al. [4] schemes for test images..

7. References

- [1] Shi, Y. Q., Li, X., Zhang, X., Wu, H. T., Ma, B.: “Reversible data hiding: Advances in the past two decades,” *IEEE Access*. 2016, **4**, pp. 3210–3237.
- [2] Tian, J.: “Reversible data embedding using a difference expansion,” *IEEE Trans. Circuits and Systems*, 2003, **13**, (8), pp. 890–893
- [3] Ni, Z., Shi, Y. Q., Ansari, N., Su, W.: “Reversible data hiding,” *IEEE Trans. Circuits and Systems*, 2006, **16**, (3), pp. 354–362
- [4] Sachnev, V., Kim, H. J., Nam, J., Suresh, S., Shi, Y. Q.: “Reversible watermarking algorithm using sorting and prediction,” *IEEE Trans. Circuits and Systems*, 2009, **19**, (7), pp. 989–999
- [5] Luo, L., Chen, Z., Chen, M., Zeng, X., Xiong, Z.: “Reversible image watermarking using interpolation technique,” *IEEE Trans. Inf. Forensics Security*, 2010, **5**, (1), pp. 187–193
- [6] Li, X., Yang, B., Zeng, T.: “Efficient reversible watermarking based on adaptive prediction-error expansion and pixel selection,” *IEEE Trans. Image Process.*, 2011, **20**, (12), pp. 3524–3533
- [7] Zhou, J., Au, O. C.: “Determining the capacity parameters in pree-based reversible image watermarking,” *IEEE Signal Process. Lett.*, 2012, **19**, (5), pp. 287–290
- [8] Coatrieux, G., Pan, W., Cappens-Boulahia, N., Cappens, F., Roux, C.: “Reversible watermarking based on invariant image classification and dynamic histogram shifting,” *IEEE Trans. Information Forensics and Security*, 2013, **8**, (1), pp. 111–120..
- [9] Dragoi, I. C., Coltuc, D.: “Local-prediction-based difference expansion reversible watermarking,” *IEEE Trans. Image Process.*, 2014, **23**, (4), pp. 1779–1790
- [10] Dragoi, I. C., Coltuc, D.: “On local prediction based reversible watermarking,” *IEEE Trans. Image Process.*, 2015, **24**, (4), pp. 1244–1246
- [11] Thodi, D. M., Rodriguez, J. J.: “Expansion embedding techniques for reversible watermarking,” *IEEE Trans. Image Proc.*, 2007, **16**, (3), pp. 721–730
- [12] Lin, S.-J., Chung, W.-H.: “The scalar scheme for reversible information-embedding in gray-scale signals: Capacity evaluation and code constructions,” *IEEE Trans. Inf. Forensics Security*, 2012, **7**, (4), pp. 1155–1167
- [13] Zhang, X.: “Reversible data hiding with optimal value transfer,” *IEEE Trans. Multimedia*, 2013, **15**, (2), pp. 316–325
- [14] Hu, X., Zhang, W., Hu, X., Yu, N., Zhao, X., Li, F.: “Fast estimation of optimal marked-signal distribution for reversible data hiding,” *IEEE Trans. Information Forensics and Security*, 2013, **8**, (5), pp. 779–788
- [15] Zhang, W., Hu, X., Li, X., Yu, N.: “Recursive histogram modification: Establishing equivalency between reversible data hiding and lossless data compression,” *IEEE Trans. Image Process.*, 2013, **22**, (7), pp. 2775–2785
- [16] Zhang, W., Hu, X., Li, X., Yu, N.: “Optimal transition probability of reversible data hiding for general distortion metrics and its applications,” *IEEE Trans. Image Process.*, 2015, **24**, (1), pp. 294–304
- [17] Kalker, T., Willems, F. M. J.: “Capacity bounds and constructions for reversible data-hiding,” in *Proc. Int. Conf. Digit. Signal Process*, Santorini, Greece, Greece, July 2002, pp. 71–76.
- [18] Ma B., Shi, Y. Q.: “A reversible data hiding scheme based on code division multiplexing,” *IEEE Trans. Information Forensics and Security*, 2016, **11**, (9), pp. 1914–1927
- [19] Lee, S. K., Suh, Y. H., Ho, Y. S.: “Public key watermarking for reversible image authentication,” in *Proc. Int. Conf. on Image Processing*, Atlanta, GA, USA, Oct. 2006, pp. 1409–1412.
- [20] Yang C.-H., Tsai, M.-H.: “Improving histogram-based reversible data hiding by interleaving predictions,” *IET Image Process.*, 2010, **4**, (4), pp. 223–234
- [21] Li, X., Zhang, W., Gui, X., Yang, B.: “A novel reversible data hiding scheme based on two-dimensional difference-histogram modification,” *IEEE Trans. Information Forensics and Security*, 2013, **8**, (7), pp. 1091–1100
- [22] Li, X., Zhang, W., Gui, X., Yang, B.: “Efficient reversible data hiding based on multiple histograms modification,” *IEEE Trans. Information Forensics and Security*, 2015, **10**, (9), pp. 2016–2027
- [23] Wang, J., Ni, J., Zhang, X., Shi, Y.: “Rate and distortion optimization for reversible data hiding using multiple histogram shifting,” *IEEE Trans. Cybernetics*, 2017, **47**, (2), pp. 315–326
- [24] Xiao, M., Li, X., Wang, Y., Zhao, Y., Ni, R.: “Reversible data hiding based on pairwise embedding and optimal expansion path,” *Signal Processing*, 2019, **158**, pp. 210–218
- [25] Kamstra, L., Heijmans, H. J. A. M.: “Reversible data embedding into images using wavelet techniques and sorting,” *IEEE Trans. Image Proc.*, 2005, **14**, (12), pp. 2082–2090
- [26] Fallahpour, M., Sedaaghi, M. H.: “High capacity lossless data hiding based on histogram modification,” *IEICE Electron. Exp*, 2007, **4**, (7), pp. 205–210